Sensitivity analysis to the normal grid-resolution in a turbulent channel flow using large-eddy simulations

By J. Dombard AND G. Iaccarino

1. Motivation and objectives

Pressure losses are of primary importance in the design of gas turbines (Lefebvre 1999). They drive the mass-flow rate between the liner and the combustion chamber through dilution holes and the fuel-injector system and, thus, impact fundamental aspects of combustion such as mixing, cooling, flame stabilization, etc. Therefore, pressure losses must be predicted accurately to have a correct evaluation of the gas-turbine performance. In the context of numerical simulations, Large-Eddy Simulation (LES) has become a reference method for turbulent combustion in combustion chambers in the last ten years (Huang *et al.* 2003; Mare *et al.* 2004; Huang *et al.* 2006; Roux *et al.* 2005; Moureau *et al.* 2011). The main reason for this fast development is that LES has demonstrated superior performances compared to Reynolds-Averaged Navier-Stokes (RANS) simulations for capturing the correct velocity fields or hydrodynamic modes of the flow. However, LES may have some difficulties predicting correct pressure losses. For example, a numerical study of a non-reacting flow in a swirler performed by two state-of-the art LES solvers showed an over prediction of pressure losses by roughly 50% (Dombard *et al.* 2012). The complexity of this configuration (a radial swirler with four passages of air) makes it difficult to discriminate between physical and numerical causes. For example, the mesh resolution of the boundary layer may play an important role when wall laws are not used. Moreover, it is virtually impossible to be wall resolved in complex configurations since the computational cost would be too expensive. The size of the cells in the smallest passages of air and the stretching ratio are thus generally set as a rule of thumb, so that these two parameters can then be considered as uncertain.

That leads to the growing field of uncertainty quantification (UQ), which provides an interesting way to tackle this issue. In the context of non-intrusive methods, smart solutions (Iaccarino 2008; Le Maître & Knio 2010) have been developed to reduce the number of points in the uncertain spaces i.e, reducing the number of simulations but, performing several tens of runs is still not uncommon. That is the reason why most of the work in this field has been previously done with RANS solvers. However, the rising computational row power now makes LES more affordable to use in conjunction with UQ. Several works at the crossroads of non-intrusive UQ and LES have appeared the last decade. Most of them tackle non wall-bounded configurations such as homogeneous isotropic turbulence (Lucor *et al.* 2007; Meldi *et al.* 2011; Meyers *et al.* 2003; Meyers & Sagaut 2007*b*; Meyers *et al.* 2010; Viré & Knaepen 2009) or spatial jets (Meldi *et al.* 2012). These works address fundamental issues in LES such as the sensitivity to the subgrid scale (SGS) parameter, shape and width of the SGS filter, ways to separate the numerical and physical errors and sensitivity to the mesh resolution. Few studies have

tackled UQ in wall bounded flows and most of them used turbulent channel flows. Among those,

- Morinishi & Vasilyev (2001) propose and evaluate a two-parameter mixed SGS model on a range of grid resolutions in the streamwise and cross-stream directions for a friction Reynolds number, denoted Re_τ, of 395 and 1400.
- Meyers & Sagaut (2007*b*) studied the convergence of Direct Numerical Simulations (DNS) at coarse LES-like resolutions, varying the grid resolution in the streamwise and cross-stream directions at $\mathrm{Re}_\tau = 298$. It is shown that convergence is not monotonic. They identified coarse resolution Nx-Nz lines where the error on skin friction is null, revealing a skin-friction balancing mechanism: at coarse resolution the smallest scales cannot be captured properly but this loss of fine-scale strain is compensated by higher levels of velocity fluctuations, hence providing a low skin-friction error.
- Based on this result, Meyers & Sagaut (2007*a*) evaluated the effect of the LES filter shape, high pass filter, Reynolds number and resolution of the dominant turbulent scales on the performance of three SGS models on "non-friendly" grid resolution (i.e. where the skin friction error is not null without the SGS model.). They found very good results on skin friction, mean velocity profiles and spanwise velocity spectra independently of the SGS model employed, as well as an insensitivity to the Reynolds number. However, the type of cut-off filter had an impact on the velocity spectra.
- In Viré *et al.* (2011), the performance of three different SGS models are assessed in hydrodynamic and magnetohydrodynamic regimes in a turbulent channel flow with Re_τ varying from 614 to 1272. The authors show that discretization errors affect the finite-volume results in two ways: (1) the flow statistics differ from the spectral estimates in the absence of subgrid model; and (2) the eddy viscosity systematically underestimates the spectral value in the presence of a subgrid model.

Table 1 summarizes the variablity of meshes used in a couple of the above mentioned studies for the same $\mathrm{Re}_\tau = 395$. One can note that the mesh resolution has only been varied in the streamwise and/or cross stream directions for a constant discretization in the normal direction. In other words, the minimum grid spacing at the wall and the stretching ratio were fixed.

The objective of this brief is to fill that gap, that is, to perform a sensitivity analysis of the mesh resolution perpendicular to the wall (first space step from the wall and stretching ratio) in a turbulent channel at friction Reynolds number $\mathrm{Re}_\tau = 395$ (Moser *et al.* 1999).

2. Methodology

The configuration consists in a classical turbulent channel flow at friction Reynolds number $\mathrm{Re}_\tau = 395$ (Moser *et al.* 1999). As usual, $\mathrm{Re}_\tau = u_\tau h/\nu$ where u_τ, h and ν denote the friction velocity, channel half-height and molecular viscosity, respectively. The mass flow rate is determined through a static pressure gradient, $dP/dx = -\tau_w/h$, where $\tau_w = \rho u_\tau^2$ is the wall shear stress. Dimensional values are summarized in Table 2.

Simulations are performed with the LES solver AVBP, a compressible cell-vertex code for turbulent reacting two-phase flows, on both structured and unstructured hybrid meshes (www.cerfacs.fr/cfd/) (Granet *et al.* 2012; Poinsot & Veynante 2011; Roux *et al.* 2005; Selle *et al.* 2004; Wolf *et al.* 2012). Subgrid-scale turbulence is accounted for with the σ-model (Nicoud *et al.* 2011).

A special care is given in the choice of the mesh resolution. A schematic of the con-

Reference	A	B	C
N_x	[24-64]	64	30
N_y	64	64	138
N_z	[24-64]	[32-54]	50
Δx^+	[103.4-38.8]	48.6	48
Δy^+	0.6 $\sim$ 34.1	1.64 $\sim$ 13.4	1$\sim$17
Δz^+	[34.5 - 12.9]	[38.8-19.4]	10
Channel size	$2\pi h \times 2h \times \frac{2\pi}{3}h$	$2.5\pi h \times 2h \times \pi h$	$3.5h \times 2h \times 1.3h$
progression in the y-direction	hyperbolic tangent	hyperbolic tangent	geometric (stretching ratio=1.04)

TABLE 1. Variability of meshes used in three papers for the turbulent channel flow at the same $\mathrm{Re}_\tau = 395$. Refs A to C denote the papers of Morinishi & Vasilyev (2001); Meyers & Sagaut (2007*b*) and Nicoud *et al.* (2011), respectively. The notation [a -b] refers to a discrete range between a and b (i.e, a different mesh) whereas the notation a$\sim$b refers to a progression from a to b within the same mesh. N_x, N_y and N_z stand for the number of grid cells in the streamwise, normalwise and span-wise directions. Δx^+, Δy^+ and Δz^+ stand for the normalized grid spacing in classical wall units. h refers to the channel half-height.

$u_{\tau,target}$ [m.s^{-1}]	h [m]	ν [m^2.s^{-1}]	dP/dx [kg.m^{-2}.s^{-2}]	$\tau_{w,target}$ [kg.m^{-1}.s^{-2}]
$2.5 \cdot 10^{-1}$	$2.4 \cdot 10^{-2}$	$1.788 \cdot 10^{-5}$	-3.067	$7.36 \cdot 10^{-2}$

TABLE 2. Dimensional characteristics at $\mathrm{Re}_\tau = 395$.

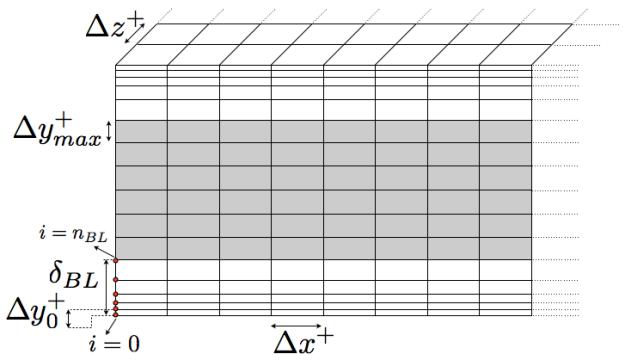

FIGURE 1. Schematic of the turbulent channel configuration. The shaded area represents the inner cells that have the baseline volume $\Delta x^+ \times \Delta y^+_{max} \times \Delta z^+$.

figuration is shown in Figure 1. The streamwise and cross-stream grid spacing in wall units are $\Delta x^+ = 48$ and $\Delta z^+ = 10$, respectively. The superscript '$^+$' classically refers to the normalization by the target DNS friction velocity $u_{\tau,target}$. The mesh discretization follows a geometric progression of stretching ratio S_r. The first grid spacing in the normal direction in wall units (hereby denoted Δy^+_0) and S_r are considered in the present study as uncertain parameters and respectively map the uncertain space $M_{\Delta y^+_0 \times S_r} = (1, 5.5, 10) \times (1.05, 1.1, 1.15, 1.2)^T$. The maximum grid spacing in the y-

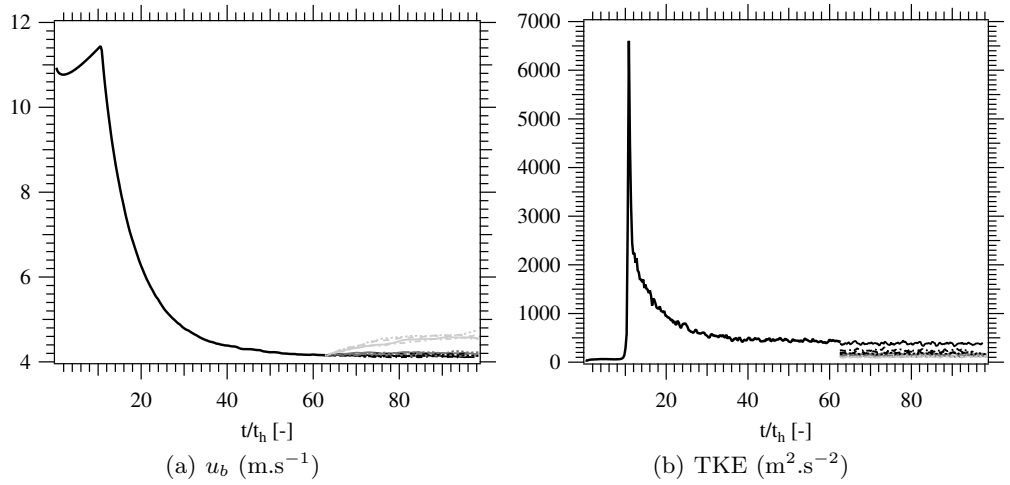

(a) u_b (m.s^{-1}) (b) TKE (m^2.s^{-2})

FIGURE 2. Temporal evolution of the bulk velocity (left) and turbulent kinetic energy (right). Time is normalized by the diffusive time. The variation of color refers to the variation in first grid spacing at the wall: $\Delta y_0^+ = 1$ (——) ; 5.5 (——) and 10 (——). The variation in the type of line refers to the stretching ratio: $S_r = 1.05$ (——) ; 1.1 (- - -) ; 1.15 (-·-) and 1.2 (·····). Spatial statistics are gathered from $t/t_h = 80$ s during 15 diffusive times.

direction is constant, fixed at $\Delta y^+_{max} = 17$. The grid progression in the normal direction is constructed such that it stops as soon as $\Delta y^+ \geq \Delta y^+_{max}$. That implies that the number of mesh cells is a function of Δy_0^+ and S_r and ranges from 180000 to 40000 cells. Note that the finest mesh, defined by the quadruplet $(\Delta x^+, \Delta y_0^+, S_r, \Delta z^+) = (48, 1, 1.05, 10)$, denoted $M_{1,1.05}$, corresponds to the one used in Nicoud *et al.* (2011).

The numerical methodology is set as follows. First, an LES is perfomed on $M_{1,1.05}$ from an initial solution consisting of a domain filled with pure air at constant temperature $T_{ref} = 300$ K, constant pressure $P_{ref} = 101325$ Pa, constant density $\rho = 1.177$ kg.m^{-3} and at constant streamwise velocity. White noise of 10% intensity is added to trigger the transition to turbulence. Statistics are run around 63 diffusive times, $t_h = h/u_\tau$, so that both bulk velocity and turbulent kinetic energy are converged, as shown in Figure 2. Then, this converged solution is used as the initial solution for the other cases. After a sufficiently-long transient time to ensure independent from the initial solution and convergence of the statistics , statistics are gathered from $t/t_h = 80$ during 15 diffusive times.

The choice of the spatial scheme is very sensitive in LES. It must be a good balance between low dissipation of the smallest turbulent structures and low dispersion of the numerical wiggles. Most of the papers about SGS models use low-dissipative high-order schemes on structured hexahedral grids. These meshes are not representative of complex configurations, in which meshes are often a mix of tetrahedral and hexahedral elements. In the latter meshes, additional numerical viscosity is often added to ensure the stability of the simulation when very low dissipative schemes are used. Consequently, the second-order in space and time scheme called Lax-Wendroff (Lax & Wendroff 1964) is preferred in the present study to other available higher-order schemes. An additional benefit is a reduced computational cost.

Finally, LES results will be compared to the finest LES, i.e, performed on the mesh

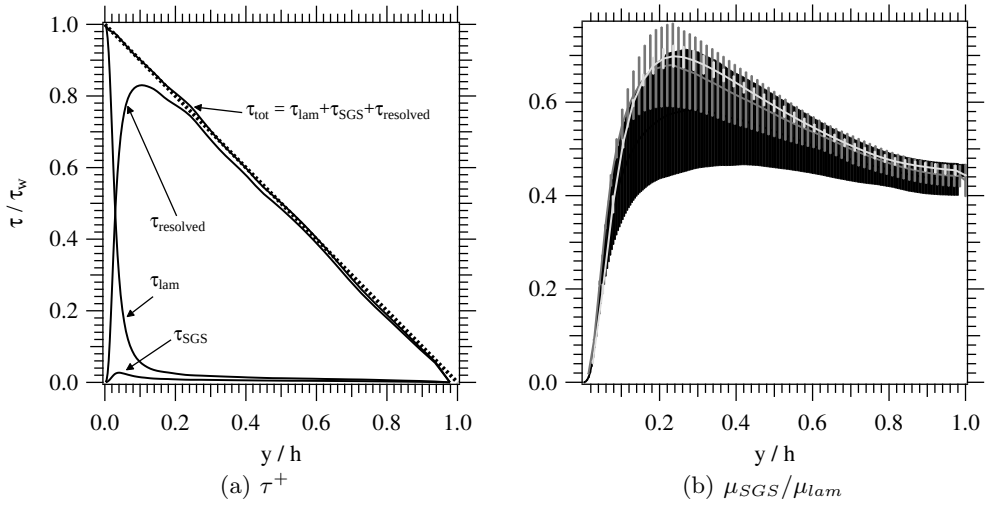

FIGURE 3. Left: Momentum conservation balance at $S_r = 1.05$ and $\Delta y_0^+ = 1$. The theoretical total shear stress ($\tau = \tau_w(1 - y/h)$) is plotted in a black thick dashed line. Right: Standard deviation of the ratio of SGS viscosity over the laminar viscosity to the stretching ratio as a function of Δy_0^+. The variation of color refers to the variation in first grid spacing at the wall: $\Delta y_0^+ = 1$ (——) ; 5.5 (——) and 10 (——).

$M_{1,1.05}$, for a fair comparison. DNS data from Moser *et al.* (1999) will be shown whenever possible but will not be used as a quantitative comparison.

3. Results

First, the effect of the stretching ratio and first grid at the wall on the SGS model is investigated. Even in such an academic configuration, it can be tedious to discriminate between the sources of error from the physics (e.g., SGS model) and from the numerics (e.g., spatial scheme) (Klein 2005). However, the impact on the SGS model can be evaluated through the momentum conservation balance and the ratio of SGS viscosity to the laminar viscosity, shown in Figure 3. As illustrated in these two figures, the contribution of the SGS model for LES is negligible: τ_{SGS}/τ_w does not exceed 0.05 and $\mu_{SGS}/\mu_{lam} < 0.8$. Then, one may consider these simulations as coarse-grid DNS. The reason why the SGS model has so few impacts is still under investigation. Note that the shear stresses are similar for the various stretching ratios and, thus, are only plotted at $S_r = 1.05$ for the sake of clarity. Conversely, both S_r and Δy_0^+ have an impact on the ratio μ_{SGS}/μ_{lam}, shown in Figure 3(b): the envelope of the standard deviation narrows when the first grid spacing at the wall increases.

We will then focus on the convergence on the skin friction coefficient since it is the main quantity of interest in channel flows. The error on the skin-friction coefficient is defined as:

$$\delta_\tau(\Delta y_0^+, S_r) = \frac{C_f(\Delta y_0^+, S_r) - C_{f,ref}}{C_{f,ref}}, \tag{3.1}$$

where $C_f = \tau_w/(\rho u_b^2)$ is the skin friction coefficient and $C_{f,ref}$ is the LES on the finest mesh. In Figure 4, the skin friction response surface to variations in Δy_0^+ and S_r (also

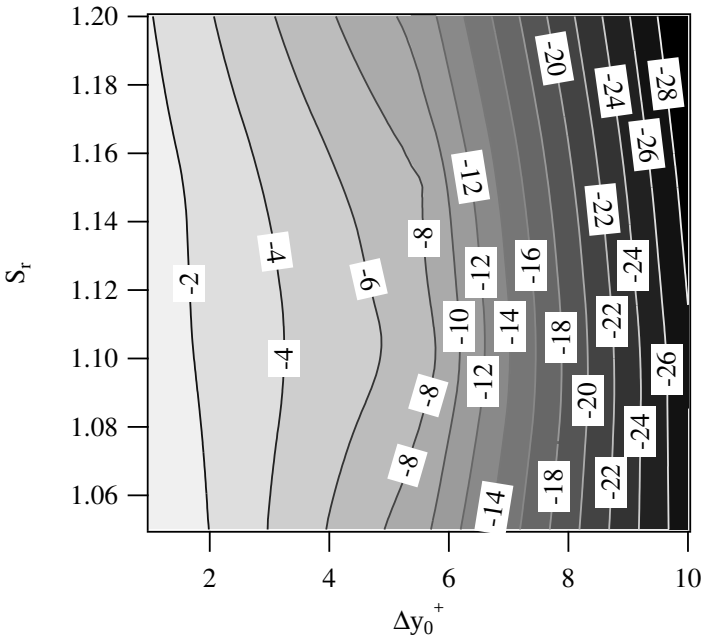

(a) $\delta_\tau(\Delta y_0^+, S_r)$

FIGURE 4. Error map of the skin friction coefficient (in %). The reference is the LES performed on the finest mesh.

referred to as the "error map") is plotted. A striking observation is that δ_τ only depends on the grid spacing at the first cell Δy_0^+. Interestingly enough, δ_τ is not monotonous as a function of Δy_0^+. It decreases sharply for $\Delta y_0^+ > 6$. Note that the number of samples in the Δy_0^+-space is minimal in the present study but this trend should be the same with more samples.

We further investigate the velocity profiles in Figure 5. Both mean and axial velocity profiles show few sensitivities to the stretching ratio. Coherently with the previous results, a clear impact of the first grid spacing at the wall is noticeable, with a jump when Δy_0^+ increases: mean velocity profiles at $\Delta y_0^+ = 5.5$ and 10 are roughly offset to the mean profile at $\Delta y_0^+ = 1$ by 10% and 30%, respectively. Observations are similar for the fluctuations of the axial velocity. Conversely, the impact of the stretching ratio is somewhat different on the fluctuations of transverse and cross-stream velocities, Figure 5(c) and 5(d), respectively.

In order to have a quantitative comparison, the L2 norms of the mean and rms velocities, defined as

$$\delta_U = \frac{\left(\int (U - U_{ref})^2 dy\right)^{1/2}}{\bar{U}}, \tag{3.2}$$

are presented in Figure 6. The reference is still the LES performed on the finest mesh, $M_{1,1.05}$. Whereas the stretching ratio has little impact on the mean velocity, it does have an effect on the velocity fluctuations for low Δy_0^+. Moreover, one can notice that the L2 norm differs as a function of the direction of the velocity: low error on u_{rms} is only found for the smallest Δy_0^+ and S_r whereas its envelope is broader for normal and cross-stream directions. As pointed out by the reviewer, this definition of the error (Equation 3.2) is

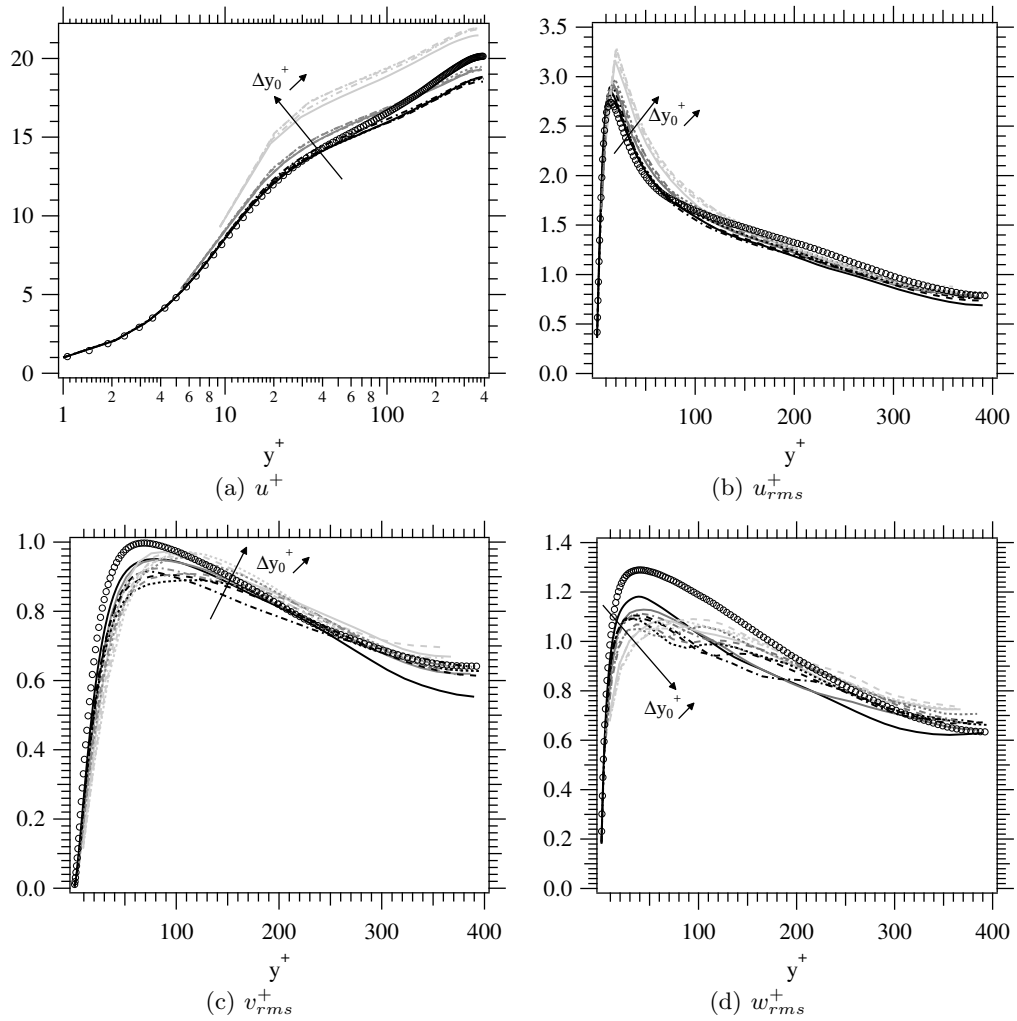

FIGURE 5. The effect of the stretching ratio and Δy_0^+ on the normalized mean and rms velocity profiles. The variation of color refers to the variation in first grid spacing at the wall: $\Delta y_0^+ = 1$ (——) ; 5.5 (——) and 10 (——). The variation in the type of line refers to the stretching ratio: $S_r = 1.05$ (——) ; 1.1 (– – –) ; 1.15 (–·–) and 1.2 (·····). Symbols refer to the DNS data (Moser *et al.* 1999). The notation $\Delta y_0^+ \nearrow$ means that the first-grid cell size at the wall increases.

somewhat misleading. Figure 5 clearly shows that the error is much larger in the mean velocity than in the rms velocities. The error norm becomes very small for the mean due to the normalization with a large value.

4. Conclusions

The sensitivity analysis to the mesh resolution in the normal direction of a turbulent channel flow at $\mathrm{Re}_\tau = 395$ has been performed using LES. In particular, the impact of the first cell size at the wall and the stretching ratio have been assessed. It was found that

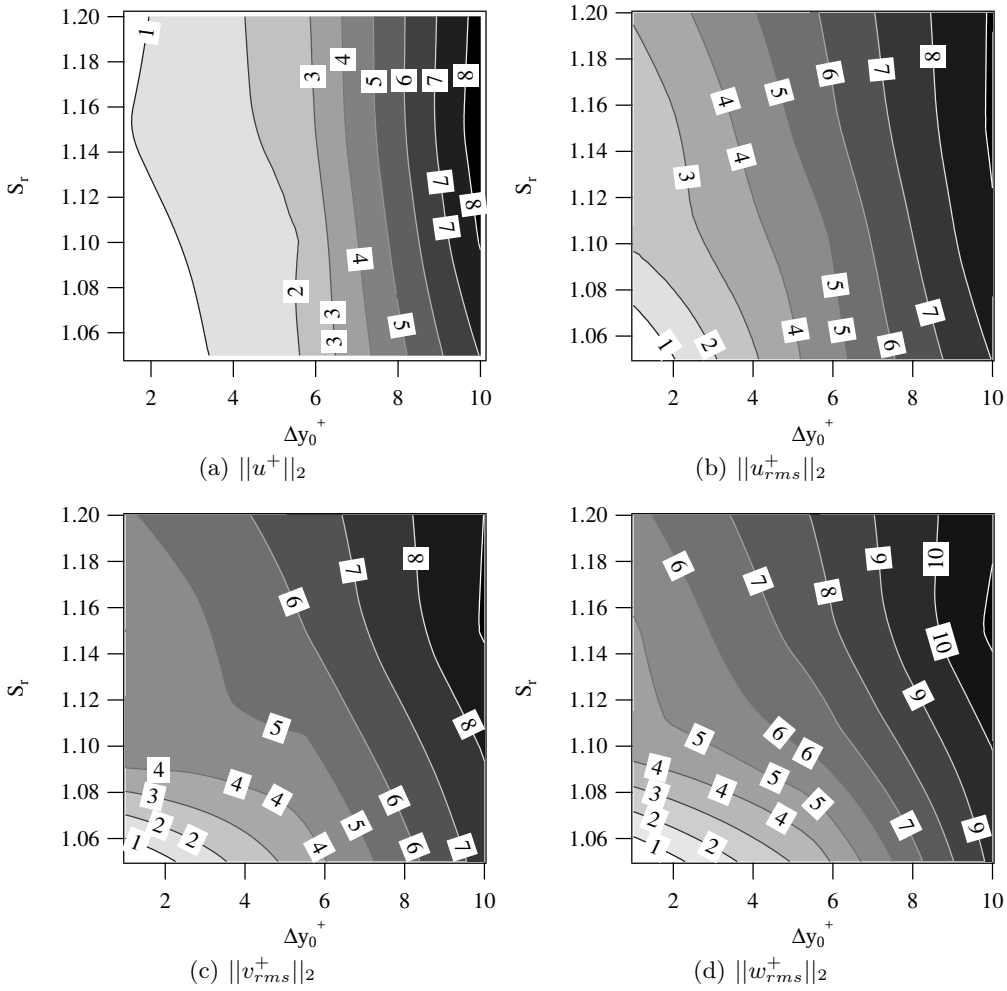

FIGURE 6. The effect of the stretching ratio and Δy_0^+ on the L2 norm of the mean and rms velocity profiles. The reference simulation is the LES performed on the finest mesh.

• the stretching ratio has few effects on the skin-friction coefficient and mean velocity whereas the first grid space at the wall highly impacts these quantities.

• the fluctuations of velocity have a different response to the stretching ratio as a function of the axis direction. Normal and cross-stream velocity fluctuations are sensitive to the stretching ratio at low first-cell sizes where it is not the case for axial velocity fluctuations.

This latter trend could have a large impact in configurations where normal and cross-stream fluctuations have an important role, like in swirl flows. The next step is a similar study in an academic swirl flow configuration like the one studied experimentally by Dellenback *et al.* (1988) or numerically by Thobois *et al.* (2005).

Acknowledgments

The authors are grateful to Mr M. Emory for his help in the mesh generation and Prof J. Larsson for useful discussions about UQ in turbulent channel flows. The authors also acknowledge Prof. F. Nicoud and Dr H. Baya-Toda for their valuable comments in the use of the σ-model.

REFERENCES

Dellenback, P., Metzger, D. & Neitzel, G. 1988 Measurement in turbulent swirling flows through an abrupt axisymmetric expansion. *AIAA J.* **13** (4), 669–681.

Dombard, J., Poinsot, T., Moureau, V., Savary, N., Staeffelbach, G. & Bodoc, V. 2012 Experimental and numerical study of the influence of small geometrical modifications on the dynamics of swirling flows. In *Proceedings of the Summer Program 2012* (ed. C. for Turbulence Research).

Granet, V., Vermorel, O., Lacour, C., Enaux, B., Duguè, V. & Poinsot, T. 2012 Large-Eddy Simulation and experimental study of cycle-to-cycle variations of stable and unstable operating points in a spark ignition engine. *Combust. Flame* **159** (4), 1562 – 1575.

Huang, Y., Sung, H. G., Hsieh, S. Y. & Yang, V. 2003 Large eddy simulation of combustion dynamics of lean-premixed swirl-stabilized combustor. *J. Propulsion & Power* **19** (5), 782–794.

Huang, Y., Wang, S. & Yang, V. 2006 Systematic analysis of lean-premixed swirl-stabilized combustion. *AIAA J.* **44** (724-740).

Iaccarino, G. 2008 Quantification of uncertainty in flow simulations using probabilistic methods. In *VKI Lecture Series 2008-09*. Von Karman Institute for Fluid Dynamics.

Klein, M. 2005 An attempt to assess the quality of large eddy simulations in the context of implicit filtering. *Flow, Turb. and Combustion* **75** (1-4), 131–147.

Lax, P. D. & Wendroff, B. 1964 Difference schemes for hyperbolic equations with high order of accuracy. *Communications on Pure and Applied Mathematics* **17**, 381–398.

Le Maître, O. & Knio, O. 2010 *Spectral methods for uncertainty quantification: with applications to computational fluid dynamics*. Springer.

Lefebvre, A. H. 1999 *Gas Turbines Combustion*. Taylor & Francis.

Lucor, D., Meyers, J. & Sagaut, P. 2007 Sensitivity analysis of large-eddy simulations to subgrid-scale-model parametric uncertainty using polynomial chaos. *J. Fluid Mech.* **585**, 255–280.

Mare, F. D., Jones, W. P. & Menzies, K. 2004 Large eddy simulation of a model gas turbine combustor. *Combust. Flame* **137**, 278–295.

Meldi, M., Lucor, D. & Sagaut, P. 2011 Is the smagorinsky coefficient sensitive to uncertainty in the form of the energy spectrum? *Phys. of Fluids* **23** (12), 125109.

Meldi, M., Salvetti, M. V. & Sagaut, P. 2012 Quantification of errors in large-eddy simulations of a spatially evolving mixing layer using polynomial chaos. *Phys. of Fluids* **24** (3), 035101.

Meyers, J., Geurts, B. J. & Baelmans, M. 2003 Database analysis of errors in large-eddy simulation. *Phys. of Fluids* **15** (9), 2740–2755.

Meyers, J., Meneveau, C. & Geurts, B. J. 2010 Error-landscape-based multiob-

jective calibration of the smagorinsky eddy-viscosity using high-reynolds-number decaying turbulence data. *Phys. of Fluids* **22** (12), 125106.

Meyers, J. & Sagaut, P. 2007*a* Evaluation of smagorinsky variants in large-eddy simulations of wall-resolved plane channel flows. *Phys. of Fluids* **19**, 095105.

Meyers, J. & Sagaut, P. 2007*b* Is plane-channel flow a friendly case for the testing of large-eddy simulation subgrid-scale models? *Phys. of Fluids* **19**, 1–4.

Morinishi, Y. & Vasilyev, O. V. 2001 A recommended modification to the dynamic two-parameter mixed subgrid scale model for large eddy simulation of wall bounded turbulent flow. *Phys. of Fluids* **13** (11), 3400–3410.

Moser, R., Kim, J. & Mansour, N. 1999 Direct numerical simulation of turbulent channel flow up to $Re_\tau = 590$. *Phys. of Fluids* **11** (4), 943–945.

Moureau, V., Domingo, P. & Vervisch, L. 2011 From large-eddy simulation to direct numerical simulation of a lean premixed swirl flame: Filtered laminar flame-pdf modeling. *Combust. Flame* **158** (7), 1340–1357.

Nicoud, F., Toda, H. B., Cabrit, O., Bose, S. & Lee, J. 2011 Using singular values to build a subgrid-scale model for large eddy simulations. *Phys. of Fluids* **23** (8), 085106.

Poinsot, T. & Veynante, D. 2011 *Theoretical and Numerical Combustion*. Third Edition (www.cerfacs.fr/elearning).

Roux, S., Lartigue, G., Poinsot, T., Meier, U. & Bérat, C. 2005 Studies of mean and unsteady flow in a swirled combustor using experiments, acoustic analysis and large eddy simulations. *Combust. Flame* **141**, 40–54.

Selle, L., Lartigue, G., Poinsot, T., Koch, R., Schildmacher, K.-U., Krebs, W., Prade, B., Kaufmann, P. & Veynante, D. 2004 Compressible large-eddy simulation of turbulent combustion in complex geometry on unstructured meshes. *Combust. Flame* **137** (4), 489–505.

Thobois, L., Rymer, G., Souleres, T., Poinsot, T. & Van den Heuvel, B. 2005 Large-eddy simulation for the prediction of aerodynamics in IC engine. *Int. J. Vehicle Des.* **39** (4), 368–382.

Viré, A. & Knaepen, B. 2009 On discretization errors and subgrid scale model implementations in large eddy simulations. *J. Comput. Phys.* **228** (22), 8203 – 8213.

Viré, A., Krasnov, D., Boeck, T. & Knaepen, B. 2011 Modeling and discretization errors in large eddy simulations of hydrodynamic and magnetohydrodynamic channel flows. *J. Comput. Phys.* **230** (5), 1903 – 1922.

Wolf, P., Balakrishnan, R., Staffelbach, G., Gicquel, L. & Poinsot, T. 2012 Using LES to study reacting flows and instabilities in annular combustion chambers. *Flow, Turb. and Combustion* **88**, 191–206, 10.1007/s10494-011-9367-7.